Electronic Supplementary Material (ESI) for Inorganic Chemistry Frontiers.

pH-controlled Assembling of POM-Based Metal-Organic Frameworks for Use as Supercapacitors and Efficient Oxidation Catalysts for Various Sulfides

Yujiao Hou,* Peilin Han, Like Zhang, Hao Li, Zhihong Xu

Key Laboratory of Chemo/Biosensing and Detection, College of Chemical and Materials Engineering, Xuchang University, Xuchang 461000, P. R. China

Corresponding author. E-mail address: Houyj@xcu.edu.cn

I. Supplementary experiments

Materials and methods

We used chemicals that were commercially purchased without further purification ($(NH_4)_6Mo_7O_{24}$/bty/$CuCl_2 \cdot 2H_2O$/H_3BO_3 were purchased from Energy Chemical and J&K Chemicals; Methyl phenyl/1-Methyl-4-(methylthio)benzene/1-Methoxy -4-(methylthio)benzene/4-Chlorothioanisole/4-Fluorothioanisole/4-Nitrylhioanisole/ benzyl sulfide /phenyl sulfide were purchased from Aladdin and Sigma-Aldrich). Elemental analyses (H and N) were performed on a Perkin-Elmer 2400 CHN elemental analyzer; Mo, Cu and B were analyzed on a PLASMA-SPEC (I) ICP atomic emission spectrometer. We detected the IR spectra using KBr pellets as the background in the range 400–4000 cm^{-1} on an Alpha Centaur FT/IR spectrophotometer. TG analyses were performed in flowing N_2 at a heating rate of 10°C min^{-1} on a Perkin-Elmer TGA7 instrument. The PXRD patterns of the samples were recorded on a Rigaku Dmax 2000 X-ray diffractometer with graphite monochromatized Cu-Ka radiation (λ = 0.154 nm) and 2θ varying from 5° to 50°. The diffuse reflectivity spectra were performed on finely ground samples with a Cary 500 spectrophotometer equipped with a 110 mm diameter integrating sphere, which were measured from 200 to 800 nm. Cyclic voltammetry (CV), galvanostatic charge−discharge (GCD) measurements, and electrochemical impedance spectroscopy (EIS) were carried out on a CHI660E electrochemical workstation. The GC analysis was performed with an Agilent HP6890 spectrometer with a flame ionization detector, which was used to monitor the conversion and selectivity.

GC−MS at the final time point was used to confirm the identity of the products. The GC−MS spectra were measured on an Agilent HP6890/5973MSD spectrometer.

General methods of electrochemical measurements.

The electrochemical performance was measured on a CHI660E electrochemical workstation in 0.1 M H_2SO_4 solution with traditional three-electrode system. The working electrodes were manufactured by the mixture of compounds (0.0010 g), graphite powder (0.0050 g) and polyvinylidene fluoride (PVDF, 0.0005g), which was ground in the agate mortar for 30 min and coated onto the treated carbon cloth (CC). The CC was pretreated based on the reported method. Then, the CC was dried under vacuum after adding 100 μL of N-methylpyrrolidone. The Ag/AgCl (3 M KCl) electrode was acted as a reference electrode, and a Pt wire was used as the counter electrode.

General methods for catalyzing the selective oxidation of MPS

MPS oxidation: MPS (0.25 mmol), catalysts (2.5 μmol), oxidant (30% H_2O_2, 0.4 mmol), internal standard (Naphthalene, 0.25 mmol) and solvent (Methanol: 0.5 mL) were mixed in the reaction vessel. The catalytic reaction was carried out at 45℃. After the catalytic reaction was finished, GC-FID and GC-MS were used to analyze and identify the resulting mixture.

X-ray crystallography

A Bruker Smart CCD diffractometer with Mo Kα radiation (λ = 0.71073 Å) was used to collect the crystallographic data of four compounds at 293 K or 220 K by θ and ω scan modes. The method of empirical absorption correction was adopted.

SHELXTL-97 software was used to solve the structures of **1** and **2** and refine the data.[1] In **1** and **2**, most non-H atoms are refined anisotropically, and only some of water molecules were excepted. H atoms linked to the C and N atoms were were fixed in their ideal positions. To get reasonable thermal parameters and atom sites, some commands such as “isor” and “dfix” were utilized.

The CCDC reference numbers for compounds **1** and **2** are 2205037 and 2205038.

II. FT-IR spectroscopy, UV-vis spectroscopy, PXRD and TG analysis.

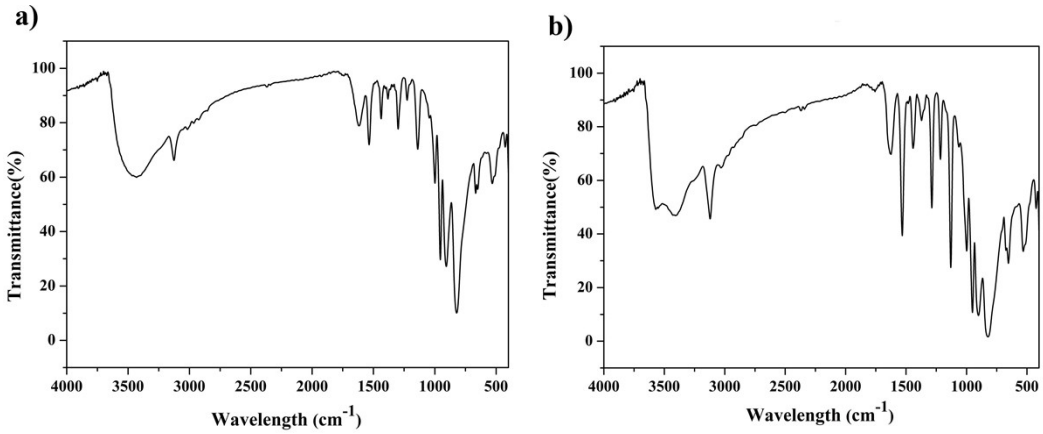

Fig. S1 IR spectra for compounds **1** and **2.**

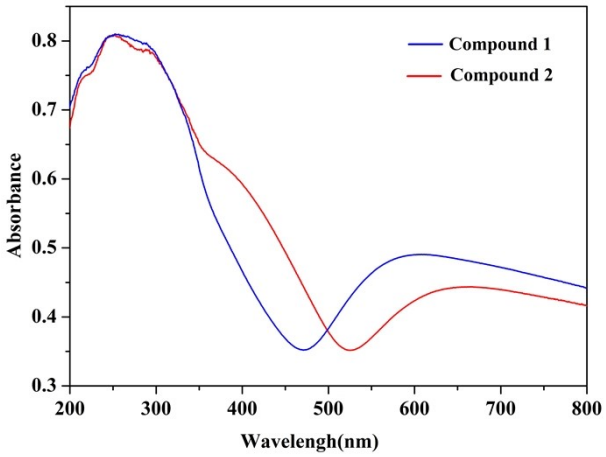

Fig. S2 UV−vis diffuse reflectance spectra of compounds **1** and **2.**

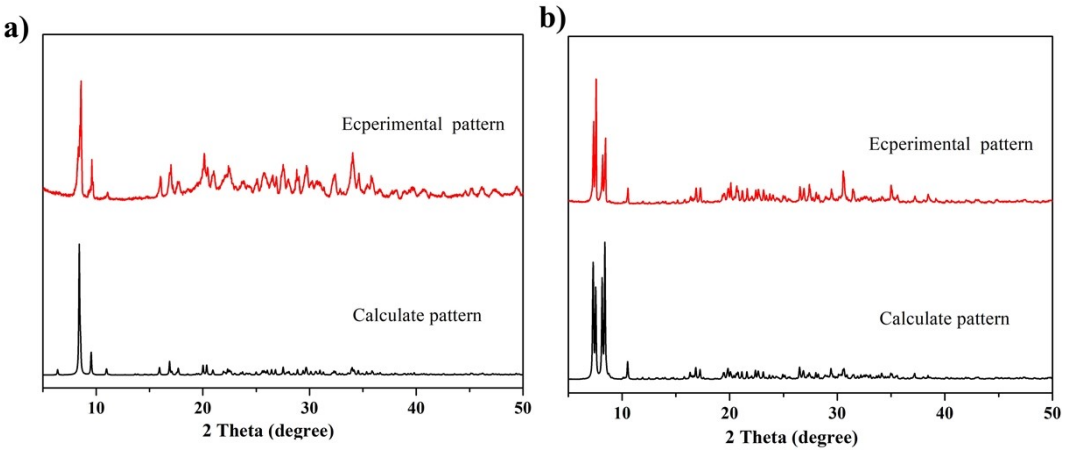

Fig. S3 a, b) The calculated and experimental PXRD patterns for compounds **1** and **2**.

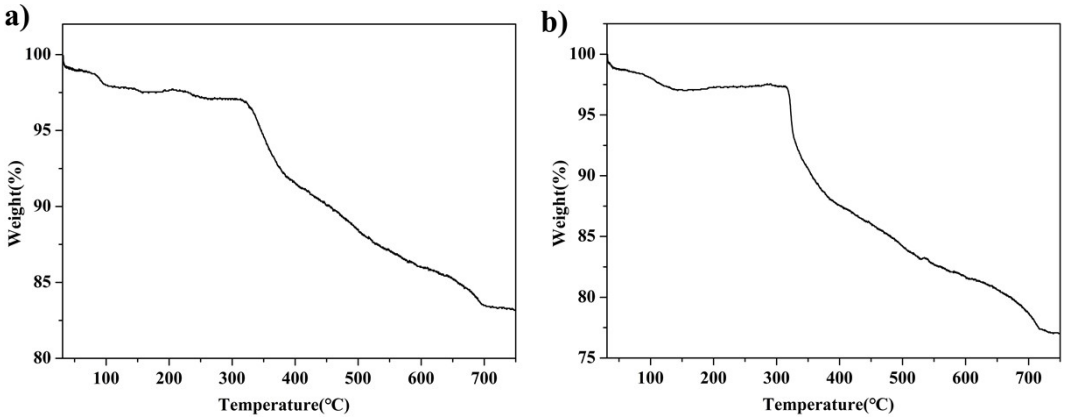

Fig. S4 Thermogravimetric plots of compounds **1** and **2**.

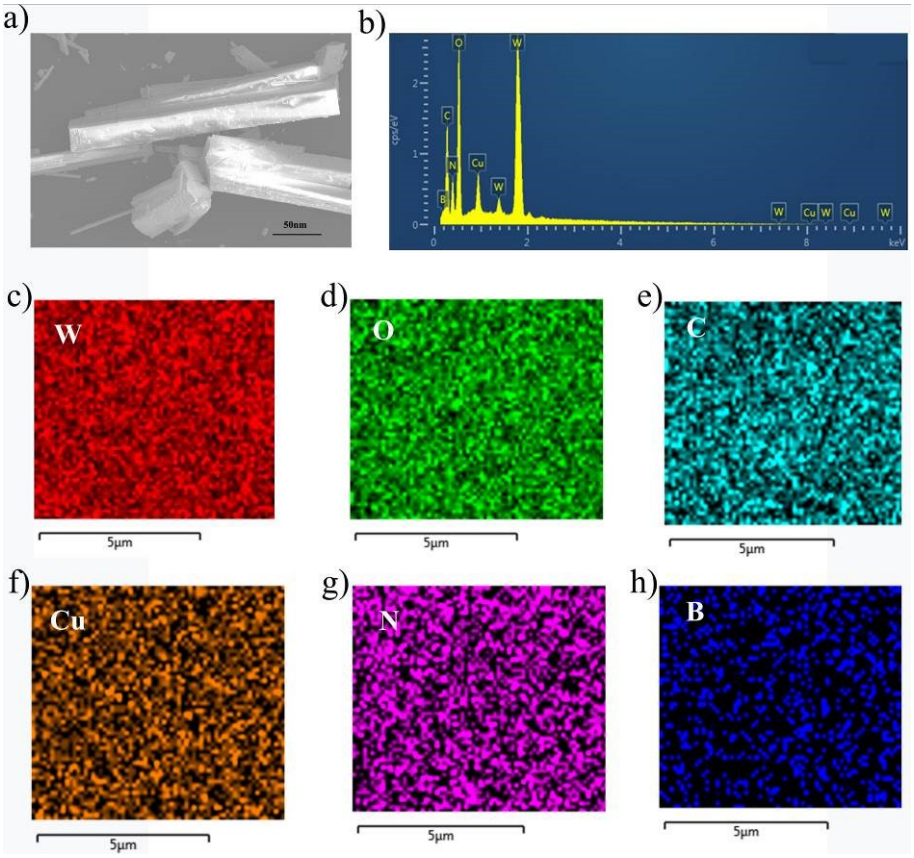

Fig. S5 a) SEM image of compound **1**; b) EDS spectrum of compound **1**; c-h) EDX elemental mapping of W, O, C, Cu, N and B in compound **1**.

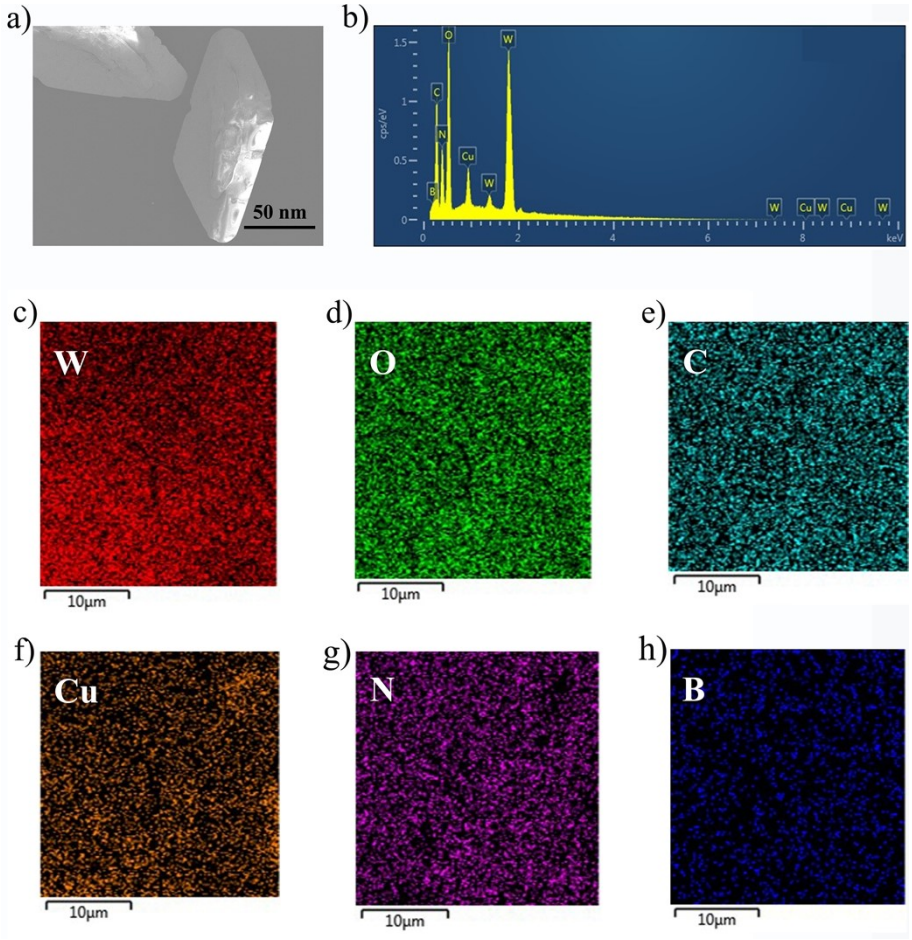

Fig. S6 a) SEM image of compound **2**; b) EDS spectrum of compound **2**; c-h) EDX elemental mapping of W, O, C, Cu, N and B in compound **2**.

III. Supplementary structure figures

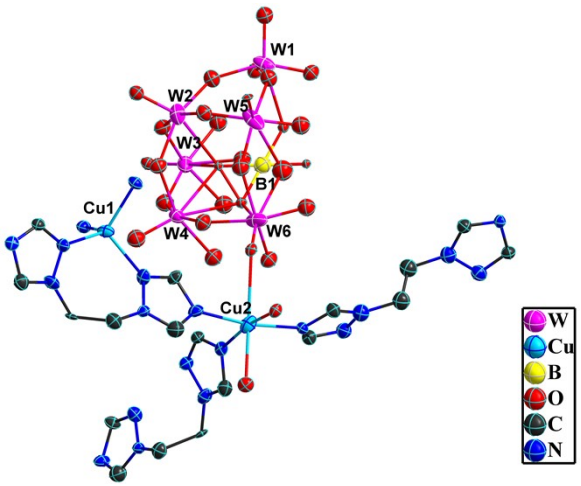

Fig. S7 ORTEP drawing of **1** with thermal ellipsoids at 50% probability. Free water molecules are omitted for clarity. (Color code: W, purple; B, yellow; Cu, light blue; O,

red; N, blue; C, black.).

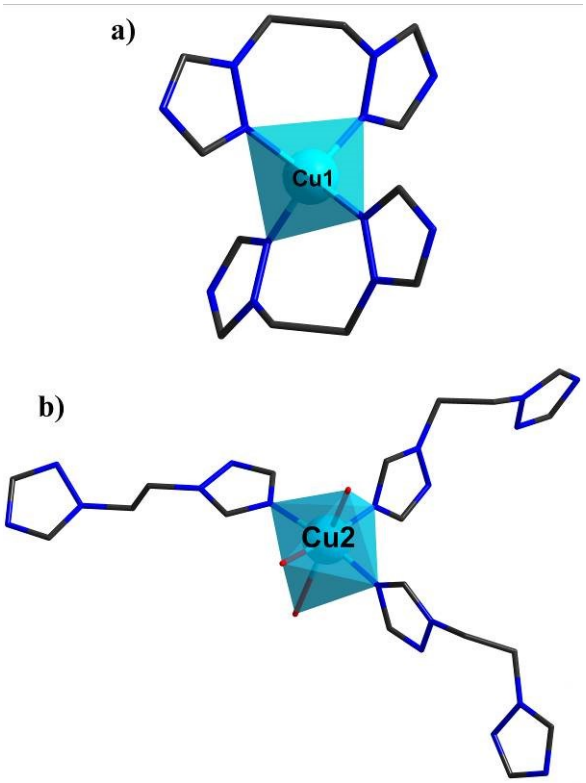

Fig. S8 a) Tetra-coordinated tetrahedral geometry of Cu1; b) Six-coordinated octahedral geometry of Cu2 in **1**. The Cu–N bond lengths are in the range from 1.976(3)- 2.048(3) Å, and the N-Cu-N angle is 102.2(18)-115.1(18)°.

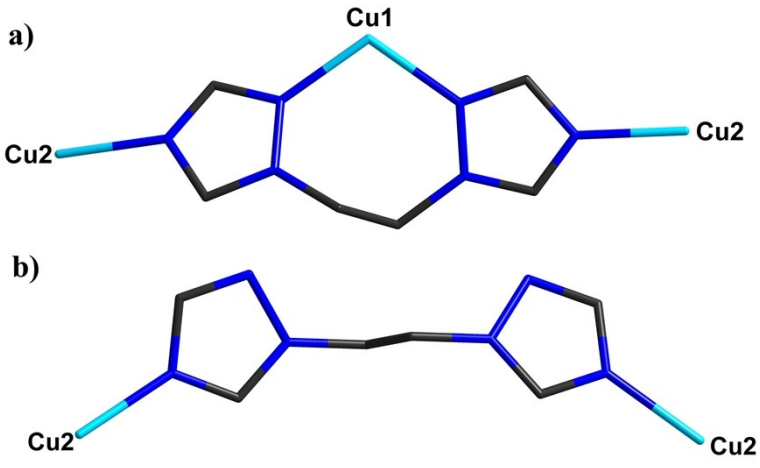

Fig. S9 a and b) The coordination modes of bty ligands in **1**.

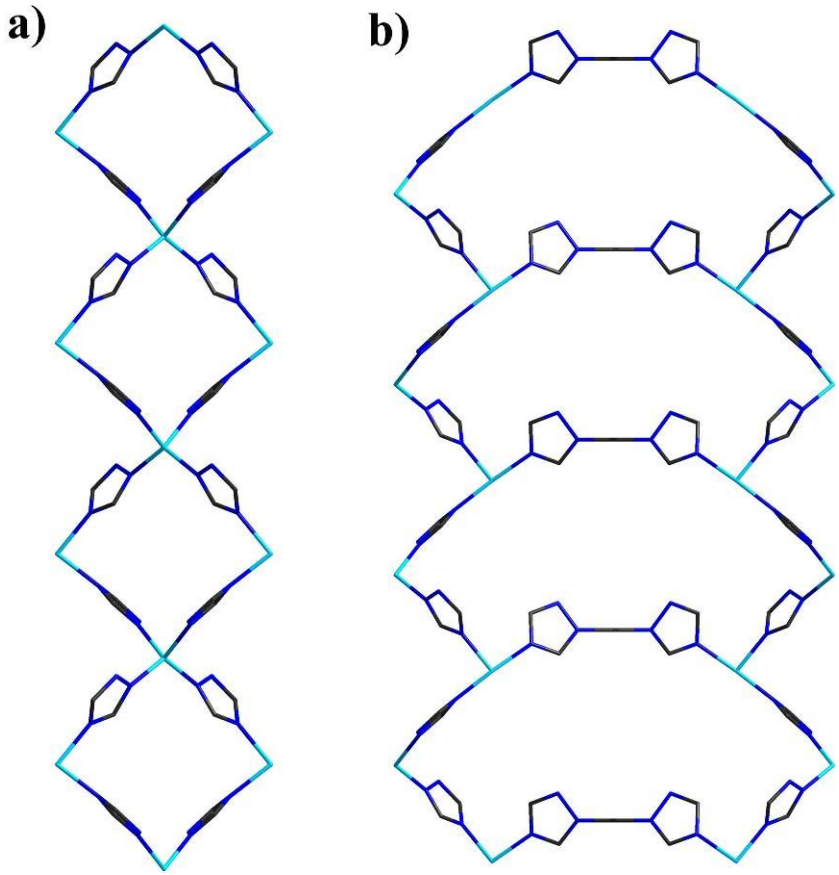

Fig. S10 a) view of 1D chain constructed from $\{Cu_4bty_4\}$ in compound **1**; b) View of 1D chain constructed from $\{Cu_6bty_6\}$ in compound **1**.

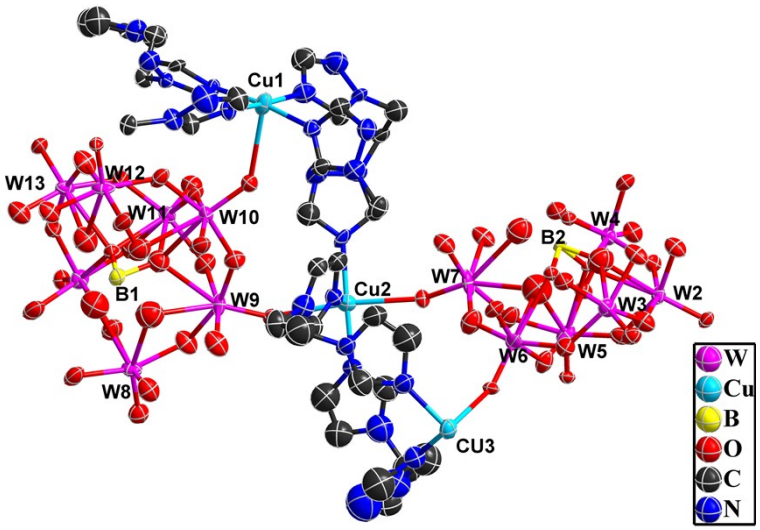

Fig. S11 ORTEP drawing of **2** with thermal ellipsoids at 50% probability. Free water molecules are omitted for clarity. (Color code: W, purple; B, yellow; Cu, light blue; O, red; N, blue; C, black.).

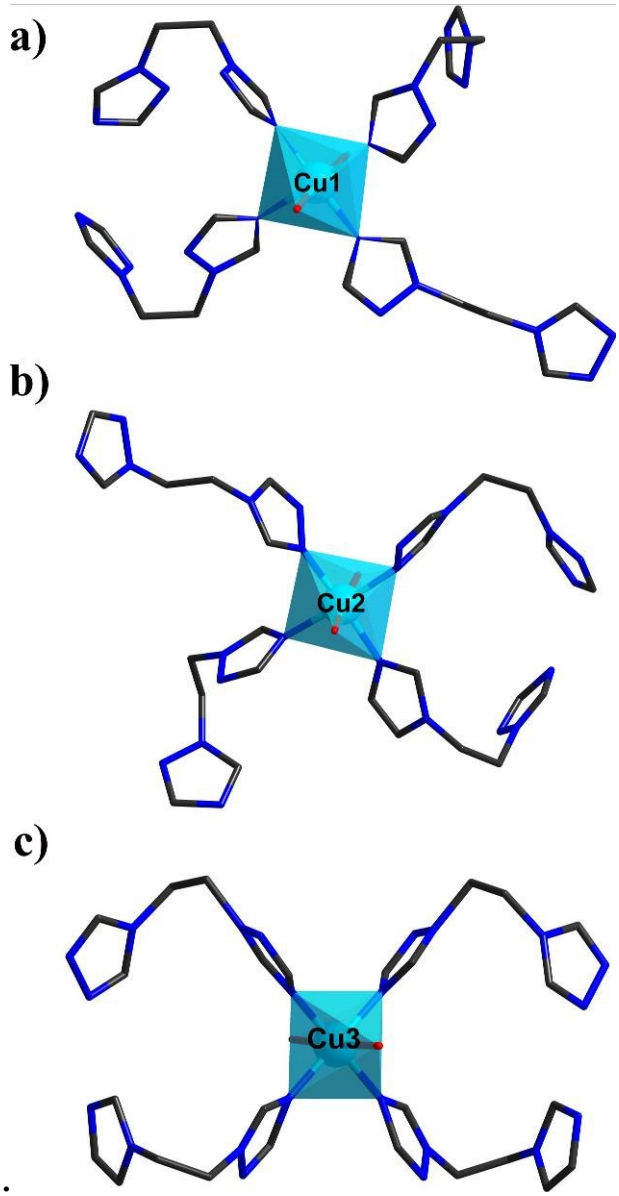

Fig. S12 a) Six-coordinated octahedral geometry of Cu1 in **2**; b) Six-coordinated octahedral geometry of Cu2 in **2**; c) Six-coordinated octahedral geometry of Cu3 in **2**. The Cu–N bond lengths are in the range from 1.980(2)-2.046(3) Å, The Cu–O bond lengths are in the range from 2.368(2)-2.460(2) Å, the N-Cu-N angle is 86.8(11)-172.2(12)° and the O-Cu-O angle is 91.2(9)-172.7(7)°.

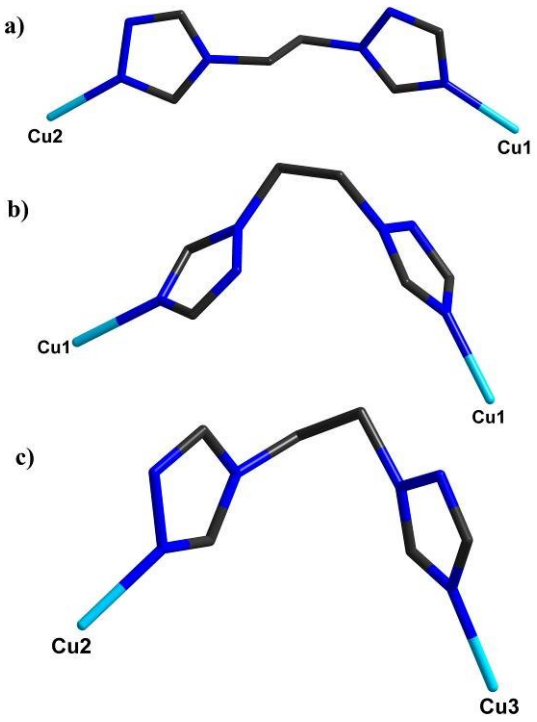

Fig. S13 a, b and c) The coordination modes of bty ligands in **2**

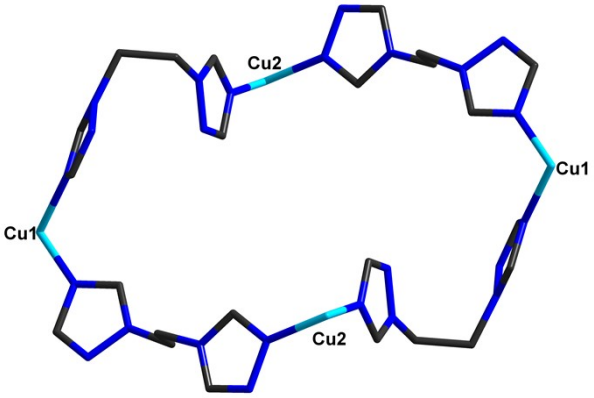

Figure S14 Ball and stick representation of the subunit $\{Cu_4bty_4\}$ in compound **2.**

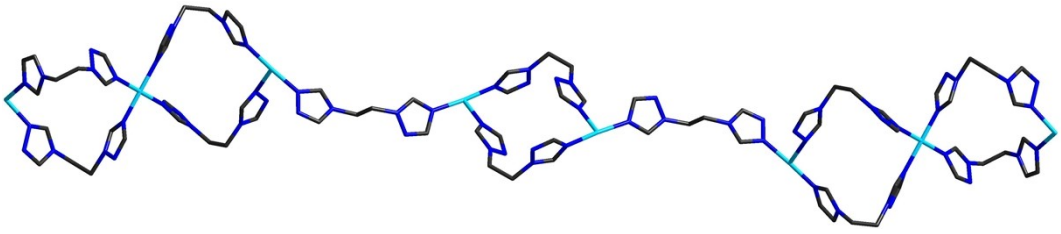

Fig. S15 view of 1D chain constructed from $\{Cu_2bty_2\}$ and $\{Cu_3bty_4\}$ in compound **2.**

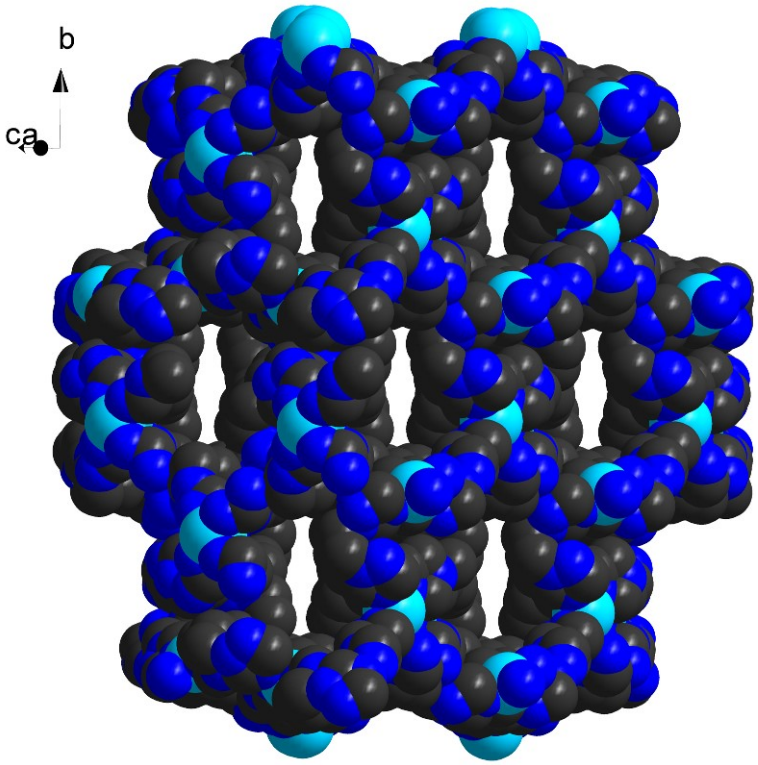

Fig. S16 The 3D space-filling framework of compound **2**.

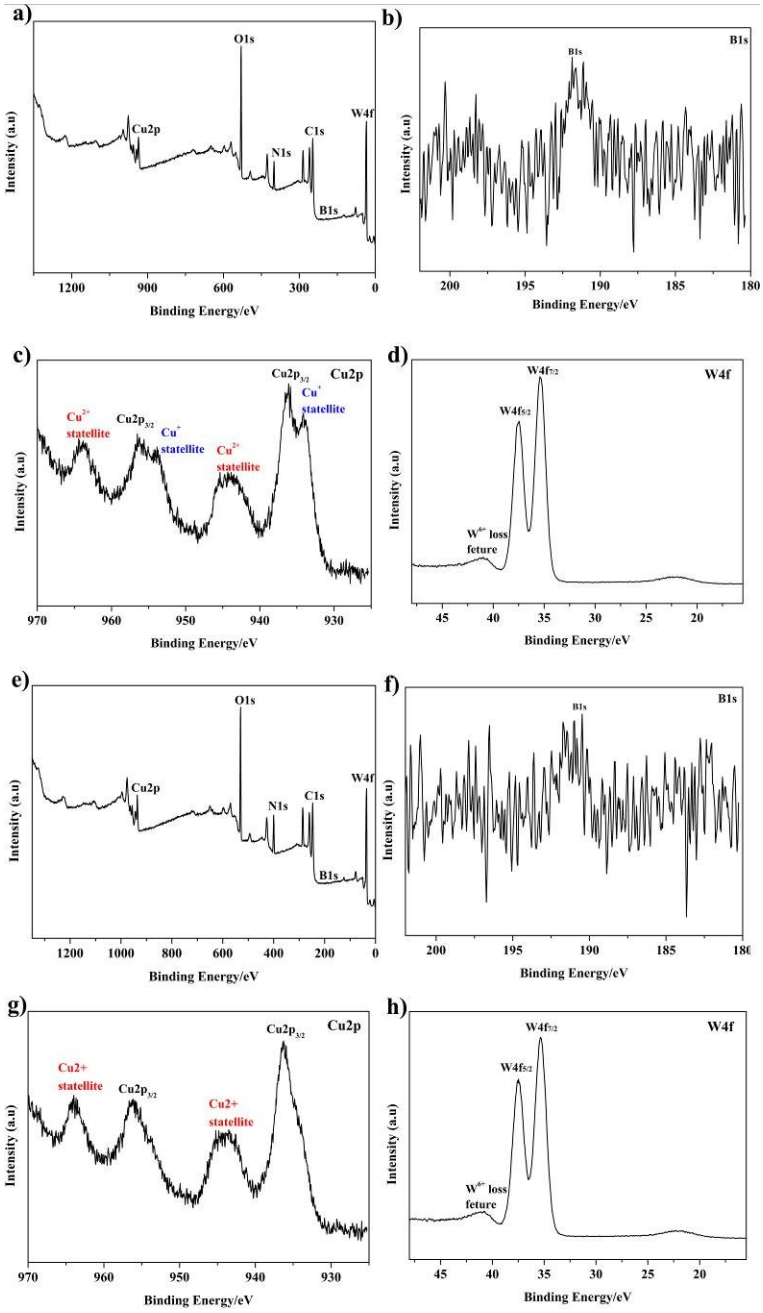

Fig. S17 a) XPS full spectrum for compound **1**; b) High-resolution scan of B1s electron in compound **1**; c) High-resolution scan of Cu2p electron in compound **1**; d) High-resolution scan of W4f electron in compound **1**; e) XPS full spectrum for compound **2**; f) High-resolution scan of B1s electron in compound **2**; g) High-resolution scan of Cu2p electron in compound **2**; h) High-resolution scan of W4f electron in compound **2**.

IV. Capacitive Performance figures

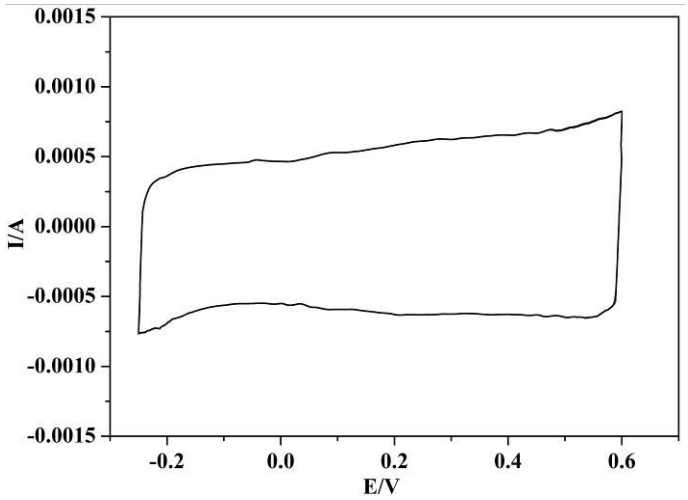

Fig. S18 CV curve of empty glassy carbon electrodes in 0.1 H_2SO_4 aqueous solution.

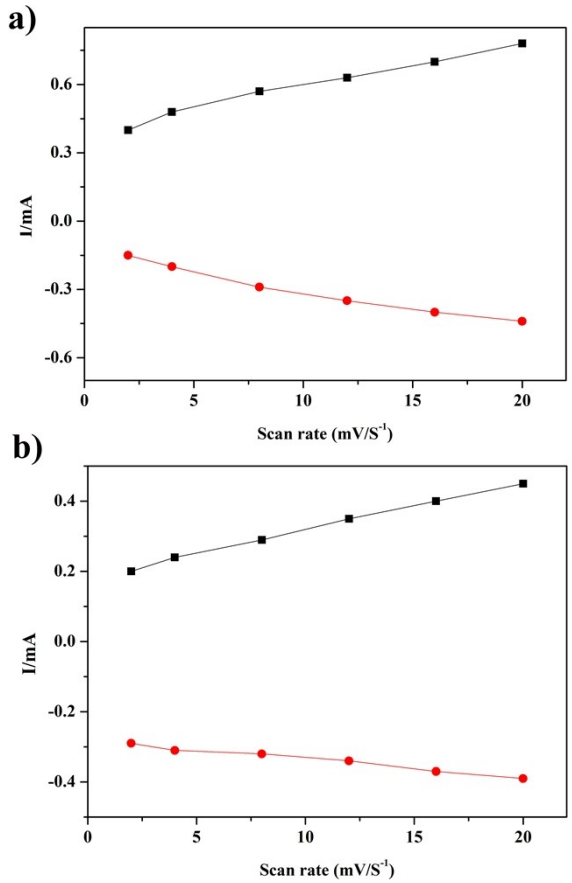

Fig. S19 a and b) Plots of the anodic and cathodic peak current vs scan rates of compound **1** and **2**.

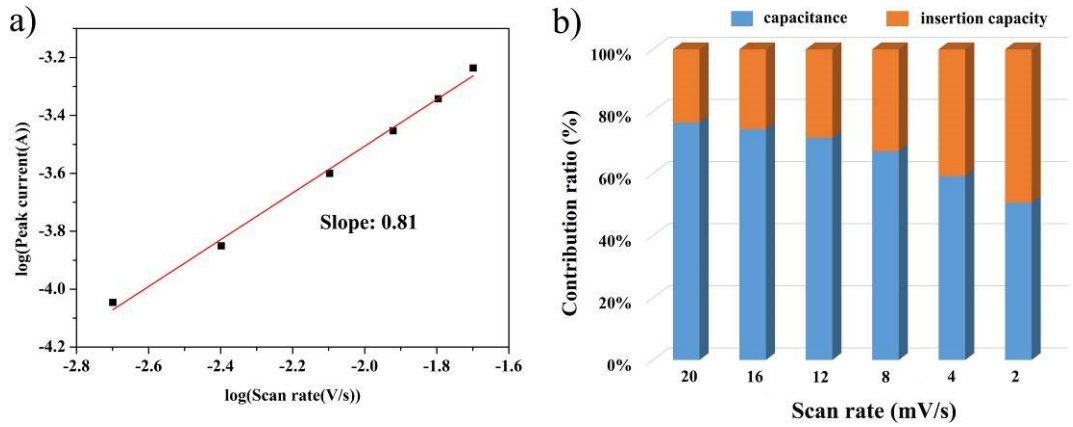

Fig. S20 a) Fitting b-value of the peak currents; b) Contribution ratio of the capacitive versus scan rate.

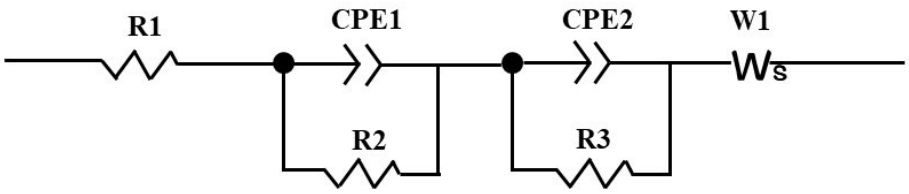

Fig. S21 The equivalent circuit of electrochemical impedance spectra of sulfur composite cathodes.

V. Catalytic oxidation study

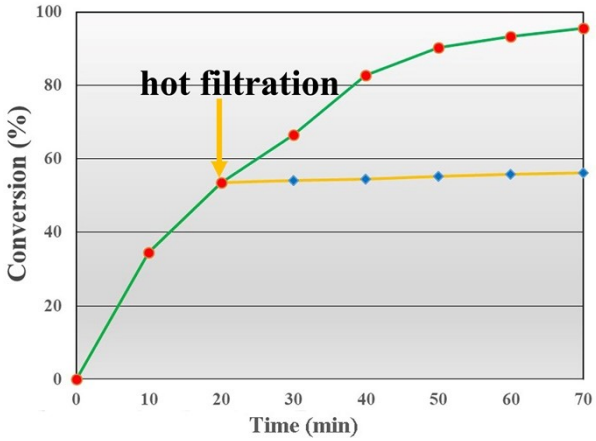

Fig. 22 The conversion of MPS oxidation for compound **2** and the hot filtration test for the oxidation of MPS.

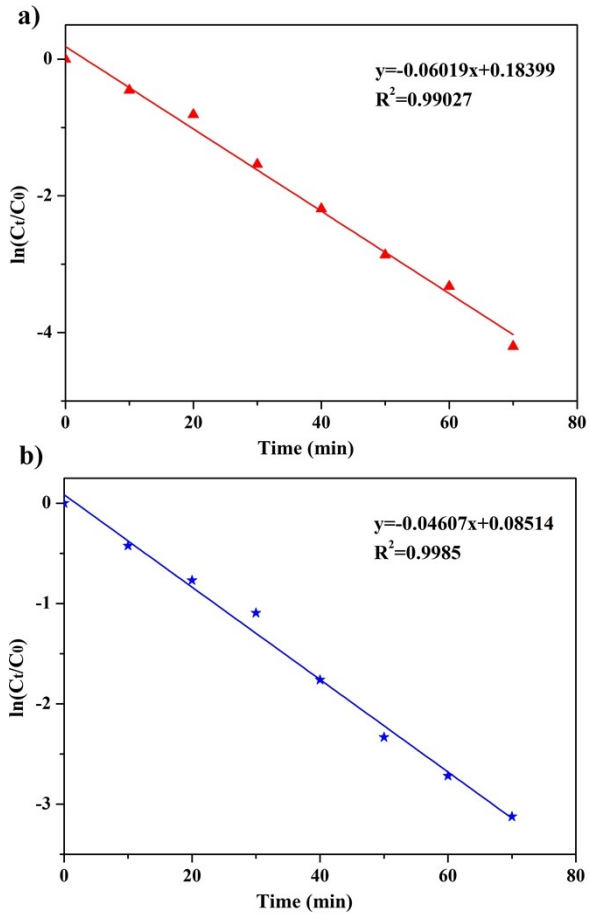

Fig. S23 a and b) Kinetic analysis of MPS oxidation for compounds **1** and **2** ($\ln(C_t/C_0)$ versus reaction time, C_t and C_0 represent the concentration of MPS at some time and the starting time).

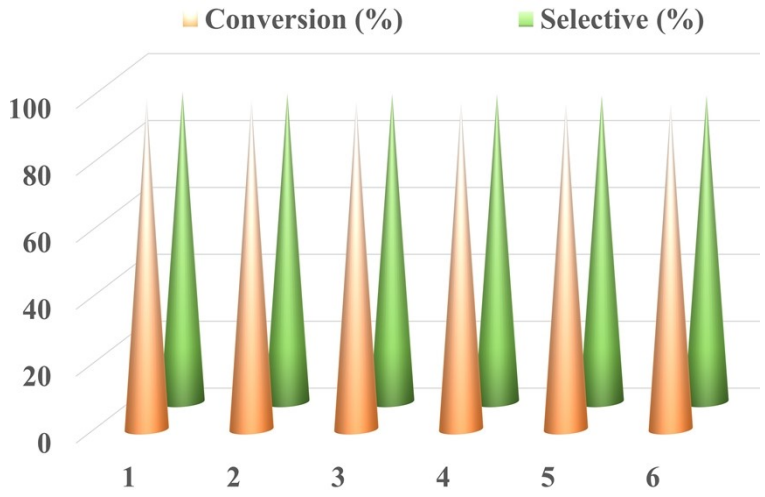

Fig. S24 Recycling of the catalytic system for the oxidation of MPS using compound **1**.

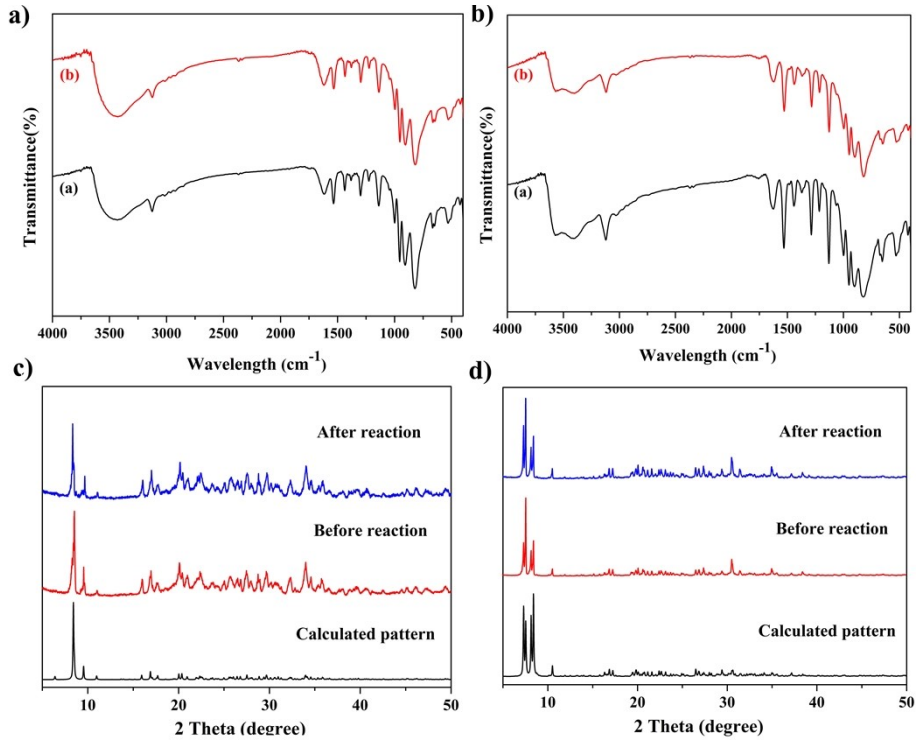

Fig. S25 a) IR spectra for **1**; b) IR spectra for **2**; c) PXRD patterns for **1**; (d) PXRD patterns for **2** before and after catalysis. In the IR spectra, the black and red lines represent the infrared absorption curves of the fresh catalyst and the catalyst recovered after the reaction, respectively. In the PXRD patterns, the red and blue lines represent PXRD patterns of the fresh catalyst and the catalyst recovered after the reaction, respectively, and the black curve is the simulated value.

Table S1. Some POM-based hybrids as electrodes materials of supercapacitors.

Electrode	C_S(F·g^{-1})	Current density(A·g^{-1})	ref
Compound **1**	214.59	0.48	This work
Compound **2**	189.17	0.48	This work
$H\{Zn_4(DIBA)_5(HPO_2)]_2$ $(\alpha\text{-}PMo_8Mo_4O_{40}Zn_2)\}$	171.17	0.5	2
$[\varepsilon\text{-}PMo_8Mo_4O_{37}(OH)_3$ $Zn_4(HDBIBA)_2]\cdot 6H_2O$	146.77	0.5	
$[Ag_{10}(C_2H_2N_3)_8][HVW_{12}O_{40}]$	93.5	1.5	3
$[Ag_{10}(C_2H_2N_3)_6][SiW_{12}O_{40}]$	47.8	1.5	
$[Ag(C_2H_2N_3)][Ag_{12}(C_2H_2N_3)_9$ $[H_2BW_{12}O_{40}]$	42.8	1.5	
$Ag_5(C_2H_2N_3)_6][H_5\subset SiMo_{12}O_{40}]$	155.0	0.5	4
$[Cu_4H_2(btx)_5(PW_{12}O_{40})_2]\cdot 2H_2O$	100.0	2	5
$[CuCu_3(H_2O)_2(btx)_5(PW_{10}W_2O$ $_{40})]\cdot 2H_2O$	82.1	2	
$[Cu_6(btx)_6(PW_9W_3O_{40})]\cdot 2H_2O$	76.4	2	
$[Ru(bpy)_3]_3PMo_{18}O_{62}\cdot nH_2O$	68	0.2	6
$H_3PMo_{12}O_{40}$/CNTs	40	0.01	7
AC/$H_3PMo_{12}O_{40}$	45	1	8
PEDOT/PMo_{12}	130.0	0.4	9
PMo_{12}/PPy	162.1	0.5	10

Table S2. Some POM-based hybrids as catalysts for MPS oxidation.

Catalyst	Oxidant	Temper. (℃)	Time (min)	Con. (%)	Sel. (%)	Refs.
Compound 1	H_2O_2	45	70	98.2	94.6	This work
Compound 2	H_2O_2	45	70	95.6	93.5	This work
{[ε-$PMo_8Mo_4O_{37}(OH)_3$] $[Zn_2(C_{10}N_2H_8)(H_2O)_2]_2\}_2\cdot 8H_2O$	H_2O_2	50	30	99	99	11
TBA2H2[Zn4(im)(Him)2][ε-PMo8VMo4VIO40]·3H2O	H_2O_2	25	10	99	99	12
$[Ni(bix)_2]\{V_4O_{11}\}$	H_2O_2	40	60	100	99	13
α-$[Cu(mIM)_4]V_2O_6$	H_2O_2	40	240	98.7	100	14
β-$[Cu(mIM)_4]V_2O_6$	H_2O_2	40	240	95.8	100	
$[Cu_3(ptz)_4][Co_2Mo_{10}]$	TBHP	40	240	99	100	15
$[Cu(bim)_2]_2[Co_2Mo_{10}]$	TBHP	40	240	98.4	95.2	
$[Ni_2(1\text{-}vIM)_7][V_4O_{12}]$	H_2O_2	45	240	96.8	98.7	16
$[Cu_2(1\text{-}vIM)_8][V_4O_{12}]$	H_2O_2	45	240	98.8	96.5	
$[Co(HDTBA)V_2O_6]$	TBHP	50	15	98	98	17
$[Ni(DTBA)_2V_2O_6]$	TBHP	50	15	100	99	
{$[Cu_8(dpyh)_4]$(α-γ-Mo_8O_{26})}(β-Mo_8O_{26})	TBHP	50	30	99	99	18

Table S3. Catalytic Activity of Different Catalysts for the Oxidation of MPS

Entry	Ca	Con (%)	Sel (%)[b]	Rection System
1	$\{BW_{12}\}$	71.2	76.5	Heterogeneous
2	$CuCl_2$	69.5	53.6	Homogeneous
3	$\{BW_{12}\}$ + $CuCl_2$ + bty	85.4	72.6	Homogeneous
4	**1**	98.2	92.6	Heterogeneous
5	**2**	95.6	91.5	Heterogeneous
6	Blank	26.8	48.6	*

[a]Reaction conditions: sulfide (0.25 mmol), Catalysts (0.8 mol%), H_2O_2 (4mmol), methanol (0.5 mL); [b]Selectivity to sulfoxides, the byproduct was sulfone.

Table S4. Crystal data and structure refinement for **1** and **2**

Complex	**1**	**2**
formula	$C_{18}H_{32}BCu_3N_{18}O_{48}W_{12}$	$C_{30}H_{44}BCu_{2.5}N_{30}O_{47}W_{12}$
formula weight	3676.16	3951.80
T (K)	293(2)	293(2)
crystal system	Orthorhombic	Monoclinic
space group	*Pccn*	*C2/c*
a (Å)	18.5405(11)	35.441(2)
b (Å)	20.7398(9)	24.1797(14)
c (Å)	16.1172(8)	23.437(3)
α (˚)	90	90
β (˚)	90	128.7785(7)
γ (˚)	90	90
U ($Å^3$)	6197.5(5)	15657(2)
Z	4	8
μ (mm^{-1})	2.527	3.353
reflections collected	93141	39842
independent reflections	6517	14196
R(int)	0.1412	0.1136
GOF on F^2	1.252	1.163
R_1[a] [I> 2σ(I)]	0.1237	0.0859
wR_2[b] [I> 2σ(I)]	0.2695	0.1841

Table S5. Selected distances (Å) and angles (˚) for **1** and **2**.

Compound **1**			
W(1)-O(6)	1.63(5)	W(1)-O(7)	2.02(5)
W(2)-O(4)	1.66(4)	W(2)-O(21)	2.37(5)
W(3)-O(9)	1.66(4)	W(3)-O(19)	2.38(5)
W(4)-O(3)	1.64(4)	W(4)-O(22)	2.11(8)
W(5)-O(2)	1.73(3)	W(5)-O(22)	2.30(8)
W(6)-O(20)	1.67(7)	W(6)-O(11)	1.86(5)
B(1)-O(21)	1.53(7)	B(1)-O(22)	1.73(8)
Cu(1)-N(8)	2.03(3)	Cu(1)-N(3)	1.99(3)
Cu(2)-O(2)	2.59(3)	Cu(2)-N(1)	2.04(3)
O(21)-B(1)-O(19)	120(3)	O(21)-B(1)-O(22)	110(3)
Compound **2**			
W(1)-O(20)	1.71(2)	W(2)-O(22)	1.88(3)
W(3)-O(35)	1.93(3)	W(4)-O(5)	1.74(2)
W(5)-O(43)	2.37(3)	W(6)-O(25)	1.91(2)
W(7)-O(12)	1.70(2)	W(8)-O(26)	1.87(3)
W(9)-O(39)	1.92(3)	W(10)-O(23)	1.90(3)
W(11)-O(38)	2.41(5)	W(12)-O(37)	1.89(3)
B(1)-O(41)	1.47(4)	B(1)-O(43)	1.56(5)
Cu(1)-N(23)	2.03(3)	Cu(1)-N(25)	1.99(2)
Cu(2)-O(11)	2.37(2)	Cu(2)-N(22)	2.05(3)
Cu(3)-N(13)	1.98(3)	Cu(3)-N(11)	2.00(3)
O(41)-B(1)-O(44)	110.2(19)	O(40)-B(1)-O(42)	108(3)

1 a) G. M. Sheldrick, *SHELXL 97, Program for Crystal Structure Refinement, University of Gőttingen,* Germany, 1997; b) G. M. Sheldrick, *SHELXL 97, Program for Crystal Structure Solution, University of Gőttingen*, Germany, 1997.

2 X. Wang, H. Li, J. F. Lin, C. Y. Wang, X. L. Wang, Capped keggin type polyoxometalate-based inorganic−organic hybrids involving in situ ligand transformation as supercapacitors and efficient electrochemical sensors for detecting Cr(VI). *Inorg. Chem.,* 2021, **60**, 19287−19296.

3 Y. Hou, H. J. Pang, C. J. Gómez-García, H. Y. Ma, X. M. Wang, L. C. Tan, Polyoxometalate Metal–Organic Frameworks: Keggin clusters encapsulated into silver-triazole nanocages and open frameworks with supercapacitor performance. *Inorg. Chem.,* 2019, **58**, 16028-16039.

4 Y. Hou, D. Chai, B. Li, H. Pang, H. Ma, X. Wang, L. Tan, Polyoxometalate-incorporated metallacalixarene@graphene composite electrodes for high-performance supercapacitors. *ACS Appl. Mater. Interfaces.,* 2019, **11**, 20845-20853.

5 D. Chai, C. J. Gómez-García, B. Li, H. Pang, H. Ma, X. Wang, Tan, L. Polyoxometalatebased metal-organic frameworks for boosting electrochemical capacitor performance. *Chem. Eng. J.,* 2019, **373**, 587-597.

6 S. Chinnathambi, M. Ammam, A Molecular hybrid polyoxometalate-organometallic moieties and its relevance to supercapacitors in physiological electrolytes. *J. Power Sources.,* 2015, **284**, 524-535.

7 M. Skunik, M. Chojak, I. A. Rutkowska, P. J. Kulesza, Improved capacitance characteristics during electrochemical charging of carbon nanotubes modified with

polyoxometallate monolayers. *Electrochim Acta.,* 2008, **53**, 3862-3869.

8 V. Ruiz, J. Suárez-Guevara, P. Gomez-Romero, Hybrid electrodes based on polyoxometalate–carbon materials for electrochemical supercapacitors. *Electrochem Commun.*, 2012, **24**, 35-38.

9 D. P. Dubal, J. Suarez-Guevara, D. Tonti, E. Enciso, P. Gomez-Romero, A high voltage solid state symmetric supercapacitor based on graphene–polyoxometalate hybrid electrodes with a hydroquinone doped hybrid gel-electrolyte. *J. Mater. Chem. A.,* 2015, **3**, 23483-23492.

10 M. Wang, Y. Yu, M. Cui, X. Cao, W. Liu, C. Wu, X. Liu, T. Zhang, Y. Huang, Development of polyoxometalate-anchored 3D hybrid hydrogel for high-performance flexible pseudo-solid-state supercapacitor. *Electrochim Acta.,* 2020, **329**, 135181.

11 Y. H. Chen, S. Z. Chang, H. Y. An, Y. Q. Li, Q. S. Zhu, H. Y Luo, Y. H. Huang. Two Polymorphic polyoxometalate-based metal−organic frameworks for the efficient synthesis of functionalized sulfoxides and detoxification of mustard gas simulants, A*CS Sustainable Chem. Eng.,* 2021, **9,** 15683−15693.

12 Y. H. Chen, H. Y An, S. Z. Chang, Y. Q. Li, Q. S. Zhu, H. Y. Luo, Y. H. Huang. A POM-based porous supramolecular framework for efficient sulfide–sulfoxide transformations with a low molar O/S ratio. *Inorg. Chem. Front.*, 2022, **9**, 3282–3294.

13 T. Y. Dang, R. H. Li, H. R. Tian, Q. Wang, Y. Lu, S. X. Liu. Tandem-like vanadium cluster chains in a polyoxovanadate-based metal–organic framework for efficient catalytic oxidation of sulfides. *Inorg. Chem. Front*., 2021, **8**, 4367–4375.

14 J. Li, X. Huang, S. Yang, Y. Xu, C. Hu, Controllable synthesis, characterization,

and catalytic properties of three inorganic−organic hybrid copper vanadates in the highly selective oxidation of sulfides and alcohols. *Cryst. Growth Des.,* 2015, **15**, 1907−1914.

15 H. An, Y. Hou, L. Wang, Y. Zhang, W. Yang, S. Z. Chang, Evans-Showell-Type polyoxometalates constructing high-dimensional inorganic-organic hybrid compounds with copper-organic coordination complexes: synthesis and oxidation catalysis. *Inorg. Chem.,* 2017, **56**, 11619−11632.

16 J. Li, C. Wei, D. Guo, C. Wang, Y. Han, G. He, J. Zhang, X. Huang, C. Hu, Inorganic-Organic hybrid polyoxovanadates based on $[V_4O_{12}]^{4-}$ or $[VO_3]^{22-}$ clusters: controllable synthesis, crystal structures and catalytic properties in selective oxidation of sulfides. *Dalton Trans.,* 2020, **49**, 14148−14157.

17 X. Wang, T. Zhang, Y. Li, J. Lin, H. Li, X.-L. Wang, In situ ligand-transformation-involved synthesis of inorganic-organic hybrid polyoxovanadates as efficient heterogeneous catalysts for the selective oxidation of sulfides. *Inorg. Chem*., 2020, **59**, 17583−17590.

18 X. L. Wang, J. Y. Zhang, Z. H. Chang, Z. Zhang, X. Wang, H. Y. Lin, Z. W. Cui, α−γ-Type $[Mo_8O_{26}]^{4-}$-Containing Metal−Organic Complex Possessing Efficient Catalytic Activity toward theOxidation of Thioether Derivatives. *Inorg. Chem.,* 2021, **60**, 3331−3337.